

Machine learning the Renyi entropy of multiple disjoint intervals with neural networks

Han-Qing Shi^{1,*} and Hai-Qing Zhang^{1,2,†}

¹*Center for Gravitational Physics, Department of Space Science,
Beihang University, Beijing 100191, China*

²*Peng Huanwu Collaborative Center for Research and Education,
Beihang University, Beijing 100191, China*

Renyi entropy with multiple disjoint intervals are computed from the improved swapping operations by two methods: one is from the direct diagonalization of the Hamiltonian and the other one is from the state-of-the-art machine learning method with neural networks. We use the paradigmatic transverse-field Ising model in one-dimension to demonstrate the strategy of the improved swapping operation. In particular, we study the second Renyi entropy with two, three and four disjoint intervals. We find that the results from the above two methods match each other very well within errors, which indicates that the machine learning method is applicable for calculating the Renyi entropy with multiple disjoint intervals. Moreover, as the magnetic field increases, the Renyi entropy grows as well until the system arrives at the critical point of the phase transition. However, as the magnetic field exceeds the critical value, the Renyi entropy will decrease since the system enters the paramagnetic phase. Overall, these results match the theoretical predictions very well and demonstrate the high accuracy of the machine learning methods with neural networks.

Keywords: Renyi Entropy, Multiple Disjoint Intervals, Machine Learning, Neural Network

I. INTRODUCTION

Entanglement maybe is the most mysterious phenomenon in the nature [1]. Entanglement entropy is one of the vast quantities to describe how the systems are entangled [2]. Among of these, Renyi entropy [3], which characterizes more information than the usual entropy, is an extension of the entanglement entropy. It provides a broader framework for measuring the uncertainty or randomness of a probability distribution and has found tremendous applications in various fields, including information theory, statistical physics, cryptography and etc [4–6].

For a given Hilbert space which is separated into two parts, Renyi entropy serves as a valuable tool for measuring the entanglement between the subsystem A and its complement. For one-dimensional critical systems, the (Renyi) entanglement entropy has been analytically studied by the conformal field theory [7–11]. However, until now there is no analytical formula of the Renyi entropy for the non-critical systems, time evolution or non-equilibrium systems. In this case, we can resort to numerical simulations. For instance, high-precision approximated states can be obtained through quantum Monte Carlo simulations [12, 13], machine learning methods [14, 15], tensor networks [16] and etc. Recently, Hastings et.al. [17] have introduced an approach to compute the Renyi entropy with one disjoint interval by evaluating the expectation value of a “swapping operator”. However, in the real systems, such as quantum many-body system [18], holography [19–21] and etc, one may need to consider the Renyi entropy with multiple disjoint intervals, rather than only one disjoint interval. Under these circumstances, it is hard to calculate the Renyi entropy from the method introduced in [17]. Therefore, it is indispensable to develop a new method to calculate the Renyi entropy with multiple disjoint intervals. In our recent paper [22], we have developed a universal approach to study the generic m -th order Renyi entropy with multiple disjoint intervals, inspired from the similarities between the “replica trick” in quantum field theory [7] and the swapping operation in quantum information theory. We dub this approach as “improved swapping operation”.

* by2030104@buaa.edu.cn

† hqzhang@buaa.edu.cn

In this paper, we will investigate the Renyi entropy with multiple disjoint intervals in the one-dimensional transverse-field quantum Ising model (TFQIM) [23] by using the improved swapping operations. In order to use the improved swapping operations provided in [22], we need to first obtain the quantum states of the system, including either exact states or numerically approximated states. We will use two different methods to prepare the ground states of the system with various magnetic fields. One method is to directly diagonalize the Hamiltonian with the singular value decomposition (SVD) method [24]; The other one is to use the state-of-the-art machine learning methods with the neural networks [14, 25, 26]. In particular, we use these two methods to study the second order Renyi entropy of two, three and four disjoint intervals in the ground states of the system by varying the magnetic fields. For simplicity, we work with the periodic boundary conditions, therefore, there will be a parity symmetry of the Renyi entropy along the size of the separations. Consequently, we find that the results obtained from the above two methods match each other very well within errors, which demonstrates that the machine learning method with neural networks is applicable for computing the Renyi entropy with multiple disjoint intervals. As the magnetic field approaches zero, the Renyi entropy is roughly a constant $\ln 2$ which is consistent with the argument that the ground state mainly contains two degenerated states: the spins all point up or down. As the magnetic field grows, the Renyi entropy will grow as well until it reaches the critical point. At the critical point the system can be described by the conformal field theory, in which only the Renyi entropy with two disjoint intervals can be expressed by analytical formula [7]. In our recent paper [22], we already checked that the results of the Renyi entropy with two disjoint intervals obtained from the improved swapping operation was perfectly consistent with the conformal field theory. This in turn ensures that our methods and computations are correct. As the magnetic field continues increasing, the system will go beyond the critical regime, and the Renyi entropy will decrease since the system now enters the paramagnetic phase. As expected, the Renyi entropy will vanish if the magnetic field goes to infinity, since there will be only one configuration in which all spins will point to solely one direction.

This paper is arranged as follows: In Section II we briefly introduce our improved swapping operation presented in our recent paper [22]; In Section III we will concisely introduce the machine learning methods with the neural networks; Then we use two different methods to study the Renyi entropy with multiple disjoint intervals in TFQIM and compare them in Section IV; Finally, we draw our conclusions and discussions in Section V. In the Appendix A we will show the detailed proof of the m -th order Renyi entropy with n multiple disjoint intervals from the improved swapping operation; In the Appendix B, we will show the details of the machine learning methods with neural networks to minimize the energy and briefly introduce the Metropolis Hastings algorithm.

II. SWAPPING OPERATION TO COMPUTE THE RENYI ENTROPY WITH n MULTIPLE DISJOINT INTERVALS

The m -th order Renyi entropy is defined as:

$$S_m = \frac{1}{1-m} \ln(\text{Tr}(\rho_A^m)), \quad (1)$$

where the reduced density matrix ρ_A is obtained by tracing the whole density matrix ρ over the complement part of A , and ρ_A^m represents the m -th power of ρ_A . It is known that in the limit of $m \rightarrow 1$, the Renyi entropy will become the von Neumann entropy S_1 [1]. In a real quantum system, due to the large dimension of the Hilbert space, directly computing the m -th power of the reduced density matrix ρ_A^m is a formidable task. Fortunately, in our recent paper [22], we have proposed a novel approach to compute the m -th Renyi entropy from the swapping operation, which transforms the computation of Renyi entropy to the evaluation of the expectation value of the swapping operator. More importantly, our approach can be applied to evaluate any order of the Renyi entropy with any number of disjoint intervals, which greatly simplifies the computation. We will concisely introduce the computation of m -th order Renyi entropy with n disjoint intervals as follows (the details can be found in the Appendix A).



FIG. 1: Schematic picture to illustrate the alternate arrangements of the intervals. The subsystem A consists of the blue disjoint intervals a_i , i.e., $A = \cup_i a_i$ in which $(i = 1, 2, \dots, n)$ while the complement part $B = \bar{A}$ contains the red parts, i.e., $B = \cup_i b_i$.

We assume that the state of the entire system can be written as $|\Psi\rangle$. The subsystem A (in blue) composes $A = \cup_i a_i$ while the complement part (in red) is $B = \cup_i b_i$ where $(i = 1, 2, \dots, n)$. Their arrangements are exhibited in the Fig.1, i.e., the disjoint parts should be alternately placed as $\{a_1 b_1 a_2 b_2 \dots a_n b_n\}$. With this partition, the state of the whole system can be described as

$$|\Psi\rangle = \sum_{\mathbf{ab}} C_{a_1 b_1 \dots a_n b_n} \otimes_{i=1}^n (|a_i\rangle |b_i\rangle), \quad (2)$$

in which $\sum_{\mathbf{ab}}$ represents $\sum_{a_1 \dots a_n; b_1 \dots b_n}$ while $C_{a_1 b_1 \dots a_n b_n}$ are the coefficients of the linear superposition. And, $|a_i\rangle |b_i\rangle$ indicate the tensor product of the basis states of the i -th subsystem of A and B respectively, while $\otimes_{i=1}^n$ represents n times of the tensor products of the states $|a_i\rangle |b_i\rangle$.

Next, in order to compute the value of $\text{Tr}(\rho_A^m)$, we need to copy the state $|\Psi\rangle$ for m times and then tensor product them together, i.e., $\otimes_{j=1}^m |\Psi^j\rangle$ in which the index j indicates the j -th replica of the state $|\Psi\rangle$.¹ Now, we can build the m -th order swapping operator $S_{\text{wap}}^{(m)}$ which will act on the m copies of the states $\otimes_{j=1}^m |\Psi^j\rangle$. The rule works like,

$$\begin{aligned} S_{\text{wap}}^{(m)} \otimes_{j=1}^m |\Psi^j\rangle &= S_{\text{wap}}^{(m)} \otimes_{j=1}^m \left[\sum_{\mathbf{a}^j \mathbf{b}^j} C_{a_1^j b_1^j \dots a_n^j b_n^j} \otimes_{i=1}^n (|a_i^j\rangle |b_i^j\rangle) \right] \\ &= \otimes_{j=1}^{m-1} \left[\sum_{\mathbf{a}^j \mathbf{b}^j} C_{a_1^j b_1^j \dots a_n^j b_n^j} \otimes_{i=1}^n (|a_i^{j+1}\rangle |b_i^j\rangle) \right] \otimes \left[\sum_{\mathbf{a}^m \mathbf{b}^m} C_{a_1^m b_1^m \dots a_n^m b_n^m} \otimes_{k=1}^n (|a_k^1\rangle |b_k^m\rangle) \right] \end{aligned} \quad (3)$$

in which $\sum_{\mathbf{a}^j \mathbf{b}^j} = \sum_{a_1^j a_2^j \dots a_n^j; b_1^j b_2^j \dots b_n^j}$. From the above procedure, we can see that the effect of the swapping operator $S_{\text{wap}}^{(m)}$ is to replace the state $|a_i^{j+1}\rangle$ in the $(j+1)$ -st replica subsystem A^{j+1} with the state $|a_i^j\rangle$ in the j -th replica subsystem A^j , i.e., $|a_i^{j+1}\rangle \rightarrow |a_i^j\rangle$. Therefore, this kind of swapping operation is done for every two adjacent replicas. However, it should be noted that the state in the first subsystem A^1 must be replaced with the state in the m -th (the last) subsystem A^m , i.e., $|a_k^m\rangle \rightarrow |a_k^1\rangle$. Since we are considering the Renyi entropy of the subsystem A , the swapping operator $S_{\text{wap}}^{(m)}$ will not act on the states $|b_i^j\rangle$ in the complement subsystem B .

Subsequently, we can compute the expectation value of the swapping operator $S_{\text{wap}}^{(m)}$ under the m copied states,

$$\begin{aligned} \langle S_{\text{wap}}^{(m)} \rangle &\equiv \langle \otimes_{j'=1}^m \Psi^{j'} | S_{\text{wap}}^{(m)} | \otimes_{j=1}^m \Psi^j \rangle \\ &= \otimes_{j'=1}^m \left[\sum_{\mathbf{a}^{j'} \mathbf{b}^{j'}} C_{a_1^{j'} b_1^{j'} \dots a_n^{j'} b_n^{j'}}^* \otimes_{i'=1}^n (\langle a_{i'}^{j'} | \langle b_{i'}^{j'} |) \right] \otimes_{j=1}^{m-1} \left[\sum_{\mathbf{a}^j \mathbf{b}^j} C_{a_1^j b_1^j \dots a_n^j b_n^j} \otimes_{i=1}^n (|a_i^{j+1}\rangle |b_i^j\rangle) \right] \\ &\quad \otimes \left[\sum_{\mathbf{a}^m \mathbf{b}^m} C_{a_1^m b_1^m \dots a_n^m b_n^m} \otimes_{k=1}^n (|a_k^1\rangle |b_k^m\rangle) \right] \\ &= \prod_{j=1}^{m-1} \sum_{\mathbf{a}^j \mathbf{b}^j} \left[C_{a_1^{j+1} b_1^j \dots a_n^{j+1} b_n^j}^* C_{a_1^j b_1^j \dots a_n^j b_n^j} \right] \times \sum_{\mathbf{a}^m \mathbf{b}^m} \left[C_{a_1^1 b_1^m \dots a_n^1 b_n^m}^* C_{a_1^m b_1^m \dots a_n^m b_n^m} \right]. \end{aligned} \quad (4)$$

¹ It should be stressed that m replicas of the state $|\Psi\rangle$ resemble the replica trick in the path integral in quantum field theory. There, people also copy the fields m times as m sheets and then connect them by some particular boundary conditions to compute the Renyi entropy [7]. Indeed, in our paper [22] we were inspired from this kind of similarity and then derived the m -th order Renyi entropy from the swapping operation.

On the other hand, we can evaluate $\text{Tr}(\rho_A^m)$ from the density matrix ρ of the whole system. The whole density matrix ρ is defined as,

$$\rho \equiv |\Psi\rangle\langle\Psi| = \sum_{\mathbf{abcd}} C_{a_1 b_1 \dots a_n b_n} C_{c_1 d_1 \dots c_n d_n}^* \otimes_{i=1}^n (|a_i\rangle|b_i\rangle) \otimes_{i'=1}^n (\langle c_{i'}|\langle d_{i'}|). \quad (5)$$

in which the sum $\sum_{\mathbf{abcd}} = \sum_{\substack{a_1, \dots, a_n; b_1, \dots, b_n; \\ c_1, \dots, c_n; d_1, \dots, d_n}}$, and $\langle c_{i'}|$ represents the conjugate basis state in the i' -th disjoint interval belonging to the subsystem A while $\langle d_{i'}|$ is the conjugate basis state in the i' -th disjoint interval belonging to the complement part B . Then, the reduced density matrix ρ_A for subsystem A is obtained by tracing out the complement subsystem B ,

$$\begin{aligned} \rho_A &= \text{Tr}_B(\rho) = \sum_{\mathbf{b}'} \otimes_{j=1}^n (\langle b'_j|) \rho \otimes_{j'=1}^n (|b'_{j'}\rangle) \\ &= \sum_{\mathbf{b}'} \sum_{\mathbf{abcd}} C_{a_1 b_1 \dots a_n b_n} C_{c_1 d_1 \dots c_n d_n}^* \otimes_{j=1}^n (\langle b'_j|) \otimes_{i=1}^n (|a_i\rangle|b_i\rangle) \otimes_{i'=1}^n (\langle c_{i'}|\langle d_{i'}|) \otimes_{j'=1}^n (|b'_{j'}\rangle) \\ &= \sum_{\mathbf{abc}} C_{a_1 b_1 \dots a_n b_n} C_{c_1 b_1 \dots c_n b_n}^* \otimes_{i=1}^n (|a_i\rangle) \otimes_{i'=1}^n (\langle c_{i'}|). \end{aligned} \quad (6)$$

Then the m -th power of the reduced density matrix ρ_A becomes,

$$\begin{aligned} \rho_A^m &= \prod_{j=1}^m \left[\sum_{\mathbf{a}^j \mathbf{b}^j \mathbf{c}^j} C_{a_1^j b_1^j \dots a_n^j b_n^j} C_{c_1^j b_1^j \dots c_n^j b_n^j}^* \otimes_{i=1}^n (|a_i^j\rangle) \otimes_{i'=1}^n (\langle c_{i'}^j|) \right] \\ &= \prod_{j=1}^{m-1} \left[\sum_{\mathbf{a}^j \mathbf{b}^j} C_{a_1^j b_1^j \dots a_n^j b_n^j} C_{a_1^{j+1} b_1^{j+1} \dots a_n^{j+1} b_n^{j+1}}^* \right] \times \sum_{\mathbf{a}^m \mathbf{b}^m \mathbf{c}^m} \left[C_{a_1^m b_1^m \dots a_n^m b_n^m} C_{c_1^m b_1^m \dots c_n^m b_n^m}^* \otimes_{k=1}^n (|a_k^1\rangle) \otimes_{k'=1}^n (\langle c_{k'}^m|) \right] \quad (7) \end{aligned}$$

Therefore, the trace of ρ_A^m becomes,

$$\begin{aligned} \text{Tr}(\rho_A^m) &= \prod_{j=1}^{m-1} \left[\sum_{\mathbf{a}^j \mathbf{b}^j} C_{a_1^j b_1^j \dots a_n^j b_n^j} C_{a_1^{j+1} b_1^{j+1} \dots a_n^{j+1} b_n^{j+1}}^* \right] \times \sum_{\mathbf{a}^m \mathbf{b}^m \mathbf{c}^m} \left[C_{a_1^m b_1^m \dots a_n^m b_n^m} C_{c_1^m b_1^m \dots c_n^m b_n^m}^* \prod_{k=1}^n (\delta_{a_k^1 c_k^m}) \right] \\ &= \prod_{j=1}^{m-1} \left[\sum_{\mathbf{a}^j \mathbf{b}^j} C_{a_1^j b_1^j \dots a_n^j b_n^j} C_{a_1^{j+1} b_1^{j+1} \dots a_n^{j+1} b_n^{j+1}}^* \right] \times \sum_{\mathbf{a}^m \mathbf{b}^m} \left[C_{a_1^m b_1^m \dots a_n^m b_n^m} C_{a_1^1 b_1^1 \dots a_n^1 b_n^1}^* \right]. \end{aligned} \quad (8)$$

From the Eq.(4) we see that the trace $\text{Tr}(\rho_A^m)$ is exactly equal to $\langle S_{\text{wap}}^{(m)} \rangle$, i.e., $\text{Tr}(\rho_A^m) = \langle S_{\text{wap}}^{(m)} \rangle$. Therefore, from the definition of the Renyi entropy (1) the computation of the m -th Renyi entropy S_m with n disjoint intervals is transformed to computing the expectation values of the swapping operator,

$$S_m = \frac{1}{1-m} \ln(\langle S_{\text{wap}}^{(m)} \rangle). \quad (9)$$

It should be stressed that the above method applies for various forms of the quantum states, such as the ground states, the excited states, the dynamical states, and etc. For simplicity, we can directly diagonalize the Hamiltonian to get the ground states of the system, then we can calculate the expectation value of the swapping operator $S_{\text{wap}}^{(m)}$ to obtain the exact value of the m -th order Renyi entropy with n multiple disjoint intervals. However, diagonalizing a Hamiltonian can only be applied for small systems. For larger systems, the dimension of the Hilbert space will be exponentially increased, which makes the diagonalization of the Hamiltonian very difficult. Fortunately, the neural network can be used to approximate the ground states of the Hamiltonian [14, 25]. At this point, one can use the quantum Monte Carlo method to sample the system's configurations of the states. As a result, even for larger systems we can still calculate the Renyi entropy of multiple disjoint intervals within the allowable errors, which greatly reduces the computational complexity of the Renyi entropy.

III. MACHINE LEARNING METHODS WITH NEURAL NETWORKS

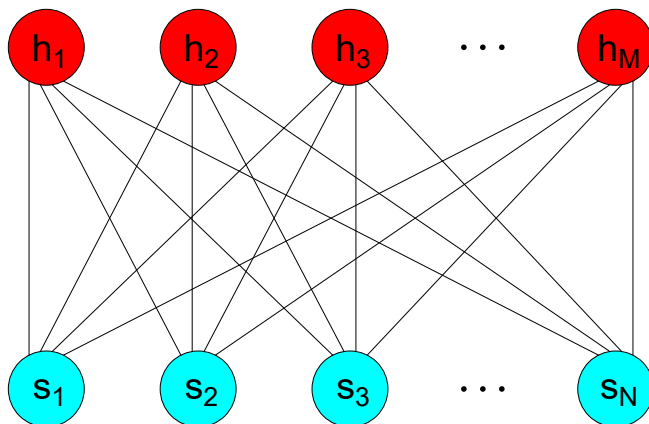


FIG. 2: Schematic figure of the structure of the RBM. The visible layer (in green) consists of N visible neurons s_j where ($j = 1, 2, \dots, N$), each of which corresponds to the spin direction $s_j = \{-1, 1\}$ at every site of the system, while the hidden layer (in red) is composed of M hidden neurons h_i where ($i = 1, 2, \dots, M$), which take values as $h_i = \{-1, 1\}$.

In this section we will introduce how to use the machine learning methods with neural networks to prepare the ground states of the quantum systems, in order to compute the expectation value of the swapping operator $\langle S_{\text{wap}}^{(m)} \rangle$. We call the quantum states prepared by the neural networks as neural-network quantum states (NQS) and written as $\Psi_{NN}(s, \mathcal{W})$, where $s = (s_1, s_2, \dots, s_N)$ denotes the quantum configurations at each site, and \mathcal{W} is the neural network parameter. NQS is a powerful approximated wave function described by a neural network, where the parameter \mathcal{W} controls the shape of the function of the system. Therefore, the goal of machine learning with the neural network is to train the system and find a suitable parameter \mathcal{W} to describe the state of the system. In our paper, we have chosen a structure that is highly compatible with quantum spin systems, i.e., the restricted Boltzmann machine (RBM) as the neural network for NQS [25, 27]. The RBM consists of two layers, one is the visible layer with N visible neurons (denoting as s_j , ($j = 1, 2, \dots, N$)) and the other layer is called the hidden layer which contains M hidden neurons (denoting as h_i , ($i = 1, 2, \dots, M$)), please refer to Fig.2. RBM have connections between the visible and hidden layers but do not have internal connections between neurons in each layer. We have chosen the number of hidden neurons to be four times than the visible neurons, i.e., $M = 4N$, which is sufficient to represent the states of the system we are studying [22, 26]. According to the structure of the neural networks, the quantum state can be described as

$$\Psi_{NN}(s, \mathcal{W}) = \sum_{\{h\}} \exp \left[\sum_j a_j s_j + \sum_i b_i h_i + \sum_{i,j} w_{ij} h_i s_j \right], \quad (10)$$

where $s = \{s_j\}$ denotes the spin configurations (or the visible neurons in Fig.2) and $\mathcal{W} = \{a_j, b_i, w_{ij}\}$ are the neural network parameters. We set the network parameters \mathcal{W} to be complex so that Ψ_{NN} can represent both the amplitudes and phases of the states. The value of s_j and h_i can be either 1 or -1 , corresponding respectively to the spin up or down. Since the hidden neurons are auxiliary structures and there are no interactions within the hidden layer, we can trace out the hidden variables with the identity $2 \cosh(x) = e^x + e^{-x}$ in the first step. Thus, Eq.(10) becomes

$$\Psi_{NN}(s, \mathcal{W}) = e^{\sum_j a_j s_j} \prod_{i=1}^M 2 \cosh[b_i + \sum_j w_{ij} s_j]. \quad (11)$$

In the machine learning methods, our goal is to find the network parameters \mathcal{W} that can represent the ground states of the system. To achieve this goal, we adopt the stochastic reconstructions (SR) method to minimize the expectation value of the system's energy $\langle E \rangle = \langle \Psi_{NN} | H | \Psi_{NN} \rangle / \langle \Psi_{NN} | \Psi_{NN} \rangle$ (The details of the SR method are provided in the Appendix B). When training NQS, the SR method can provide a rapid path to the lowest energy state in the parameter space. However, along this path, it is necessary to estimate the system's energy expectation value at each step. In order to avoid the difficulties brought by the exponentially large Hilbert space, we need to use a sampling method — the Metropolis Hastings algorithm to approximate the system's energy expectation value. The specific steps of this method are also provided in the Appendix B. Additionally, we reduce the number of independent parameters from the symmetry of the system. This improvement not only increases computational efficiency but also enhances the stability of the program. The symmetry of the system refers to the invariance of the wave function under a translational transformation \hat{T} . Therefore, we can impose the constraint $\Psi_{NN}(s, \mathcal{W}) = \Psi_{NN}(\hat{T}s, \mathcal{W})$ into the parameters \mathcal{W} to reduce the number of independent parameters.

IV. APPLICATION IN ONE-DIMENSIONAL TFQIM

In this section, we will compute the Renyi entropy with multiple disjoint intervals by the improved swapping operation. For simplicity, we consider the paradigmatic one dimensional TFQIM with periodic boundary conditions. The Hamiltonian of TFQIM with N sites is,

$$H = -J \sum_{i=1}^N (\sigma_i^z \sigma_{i+1}^z + h \sigma_i^x), \quad (12)$$

where σ_i^z and σ_i^x are respectively the z and x -components of the Pauli matrices at the i -th site, J represents the coupling strengths between the nearest-neighboring sites (we have set $J = 1$ in the computation), and h denotes the strength of transverse magnetic field along x -direction. Because of the periodic boundary conditions, the $(N + 1)$ -st site is equivalent to the first site, viz., $\vec{\sigma}_{N+1} = \vec{\sigma}_1$.

In order to get the expectation values of the swapping operator $\langle S_{\text{wap}}^{(m)} \rangle$, we need to obtain the states of the system at first. For simplicity, we will work in the ground states of the system in different phases by varying the magnetic field strength h . There exists a phase transition from the ferromagnetic to paramagnetic while the critical value of h is $h_c = 1$. For these ground states, without the loss of generality, we will compute the second order Renyi entropy S_2 with two, three and four disjoint intervals, in particular from two different methods.² The first method is to use the above machine learning methods with the neural network to prepare the approximate ground states of the systems. We choose the spin z -direction as the basis state to represent the system by using the RBM. Then, we can obtain the ground states by minimizing the expectation value of the energy with the SR method. The second method is to directly diagonalize the Hamiltonian to get the states of the system: For a finite spin chain, the dimension of Hilbert space of the Hamiltonian grows exponentially with the size of the system. We can consider the following eigenvalue equation,

$$H |\Psi_i\rangle = E_i |\Psi_i\rangle, \quad (13)$$

in which E_i and $|\Psi_i\rangle$ are respectively the i -th energy eigenvalue and eigenvector. In the TFQIM model (12), we have adopted up to $N = 24$ sites. The Hamiltonian matrices in TFQIM model are typically sparse matrices, hence, we can use the singular value decomposition (SVD) method to diagonalize the Hamiltonian matrix directly with the dimension up to $10^8 \times 10^8$ (since $2^{24} \approx 1.6777 \times 10^7$). After many trials, we find that this capacity can be readily realized on a personal computer. After diagonalizing the Hamiltonian, we then can find the eigenstates of H readily. As a result, the expectation value of the swapping operator $\langle S_{\text{wap}}^{(2)} \rangle$ can be computed exactly.

² In principle, our method from the swapping operation can be used to compute general order of the Renyi entropy with general multiple disjoint intervals. However, due to the capacity and efficiency of the computer, we begin with the simplest cases to compute S_2 with two, three and four disjoint intervals.

A. S_2 with two disjoint intervals

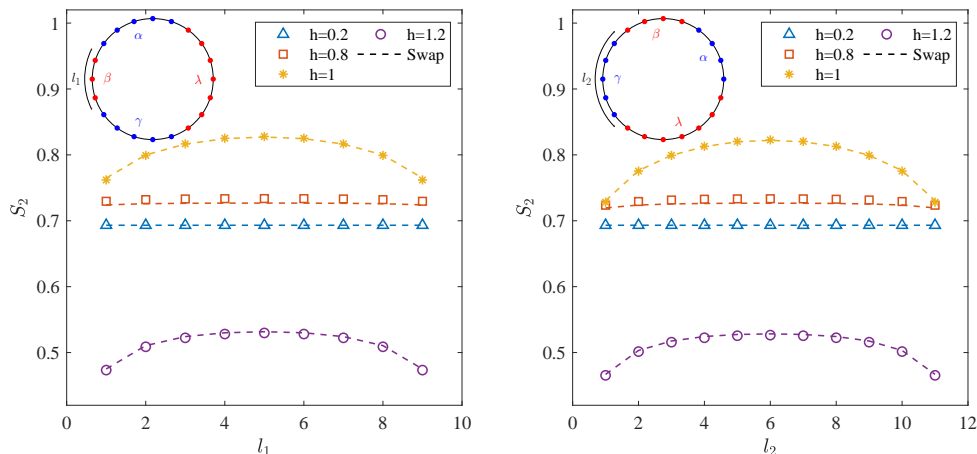


FIG. 3: (Left) Renyi entropy S_2 with two disjoint intervals ($A = \alpha \cup \gamma$) against l_1 , the length of β interval; (Right) Renyi entropy S_2 with two disjoint intervals ($A = \alpha \cup \gamma$) against l_2 , the length of γ interval. In both panels, the circles in the top-left corners are the schematic pictures to show the arrangements of the disjoint intervals. Meanwhile, different styles of the points represent the Renyi entropy obtained from the machine learning methods with neural network for various magnetic fields, while the dashed lines correspond to the diagonalization of the Hamiltonian from the SVD method. They match each other very well.

First, we consider dividing the system into four subregions. Subsystem A and its complement B each contains two disjoint intervals, please refer to the top-left corner in the left plot of Fig.3. Subsystem A (in blue) includes subregions α and γ , while the complement part B (in red) includes subregions β and λ . In this scenario, we choose the size of the whole system as 20 sites. We fix the size of each subregions α and γ to be five, and vary the separation (the length of β region which denotes as l_1) between these two subregions α and γ . The second order Renyi entropy S_2 will be computed for the subsystem A by varying the the separation l_1 with various magnetic field strengths h . In the left panel of Fig.3, we show the second order Renyi entropy S_2 against the length l_1 under different transverse magnetic field strength h . Due to the periodic boundary conditions, it is obvious to see that changing the size of β is equivalent to changing the size of λ . Therefore, there should be a parity symmetry $l_1 \leftrightarrow (10 - l_1)$ of the Renyi entropy. Hence, it greatly simplifies our computation due to this kind of parity symmetry. In plotting the left panel of Fig.3, we only plot the left part ($l_1 \leq 5$) of the picture, and then just copy the left part to the right part.³ These lines should have a parity symmetry along the vertical line $l_1 = 5$.

In the left panel of Fig.3 the data points, i.e., yellow asterisks, red squares, blue triangles and purple circles are the numerical results from the machine learning methods with neural networks. The corresponding colorful dashed lines are from the methods of diagonalizing the Hamiltonian with the SVD. We define the relative error of Renyi entropy as $\epsilon = |S_{\text{ML}} - S_{\text{SVD}}|/S_{\text{SVD}}$, where S_{ML} is the Renyi entropy from the machine learning methods while S_{SVD} is the Renyi entropy from the diagonalization of the Hamiltonian by SVD method. The relative errors for these two methods are exhibited in Table I. We can see that these two methods match each other with high precision.

From the left plot of Fig.3, we see that as the magnetic field approaches zero, i.e., $h = 0.2$, the entropy tends to a constant $\ln 2 \approx 0.69$ since in this case the system is mainly in the ferromagnetic two degenerated ground states, which have two spin configurations $|\uparrow\uparrow \cdots \uparrow\rangle$ and $|\downarrow\downarrow \cdots \downarrow\rangle$ [7]. Then the Renyi entropy will increase with the magnetic field until it reaches its maximum at the critical magnetic field $h_c = 1$. At the critical point the system is in conformal field theory, from which one can take advantage of the four point correlation functions to analytically describe the Renyi entropy

³ In the following figures, we also use this kind of strategy to plot them.

$h \backslash l_1$	1	2	3	4	5
0.2	3.89×10^{-6}	4.27×10^{-6}	4.36×10^{-6}	4.38×10^{-6}	4.39×10^{-6}
0.8	7.51×10^{-3}	8.54×10^{-3}	9.05×10^{-3}	9.31×10^{-3}	9.39×10^{-3}
1.0	3.74×10^{-3}	9.06×10^{-4}	3.21×10^{-4}	8.01×10^{-4}	9.62×10^{-4}
1.2	3.52×10^{-3}	3.52×10^{-3}	3.56×10^{-3}	3.58×10^{-3}	3.57×10^{-3}

TABLE I: The relative errors ϵ between the machine learning methods and the SVD methods for computing S_2 with two disjoint intervals. The first row represents the separation size l_1 while the first column represents the magnetic field strength h . This table corresponds to the left plot of Fig.3.

[8, 9, 11]. Indeed, in our recent paper we have compared our results from the improved swapping operation with those from the conformal field theory, and found that they matched each other very well [22]. Here, we will not show the analytical results from the conformal field theory again. At the critical point, S_2 increases with l_1 until it reaches the symmetry axis $l_1 = 5$. As the magnetic field h exceeds the critical value, for instance $h = 1.2$, the entropy will decrease compare to those at the critical point, since now the system enters the paramagnetic phase. If $h \rightarrow \infty$, the Renyi entropy will vanish as expected, because there will be only one configuration that all the spins will point to the x -direction [7].

In the right panel of Fig.3, we keep the size of the regions α and β as four, respectively. Then we change the size of γ , which is denoted as l_2 . Please be noted that in this case the subsystem A is still composed of the blue subregions, i.e., $A = \alpha \cup \gamma$. The relationship between Renyi entropy S_2 and the size of γ is shown in the right plot of Fig.3. As before, due to the periodic boundary conditions, there is also a parity symmetry $l_2 \leftrightarrow (12 - l_2)$. In the right plot, the data points, i.e., yellow asterisks, red squares, blue triangles and purple circles are the numerical results from the machine learning methods with neural networks, while the corresponding colorful dashed lines are from the the SVD methods. The relative errors ϵ between the two methods are shown in the Table II, from which we can see that these two methods align with each other very well.

$h \backslash l_2$	1	2	3	4	5	6
0.2	3.83×10^{-6}	4.23×10^{-6}	4.33×10^{-6}	4.37×10^{-6}	4.38×10^{-6}	4.38×10^{-6}
0.8	5.71×10^{-3}	7.36×10^{-3}	8.28×10^{-3}	8.84×10^{-3}	9.14×10^{-3}	9.24×10^{-3}
1.0	3.24×10^{-3}	9.36×10^{-4}	2.37×10^{-6}	4.47×10^{-4}	6.37×10^{-4}	6.86×10^{-4}
1.2	3.18×10^{-3}	3.31×10^{-3}	3.44×10^{-3}	3.53×10^{-3}	3.57×10^{-3}	3.59×10^{-3}

TABLE II: The relative errors ϵ between the machine learning methods and the SVD methods for computing S_2 with two disjoint intervals. The first row represents the size of γ , i.e. l_2 , while the first column represents the magnetic field strength h . This table corresponds to the right plot of Fig.3.

As before, we see that when h is small as $h = 0.2$, the Renyi entropy is roughly a constant $\ln 2$. When h increases the entropy increases as well until it arrives at the maximum when the system is at the critical point of the phase transition. Then we continue increasing the magnetic field, the system will go beyond the critical regime and enters the paramagnetic phase. In this case the Renyi entropy S_2 will decrease as the results for $h = 1.2$ shows. As expected, when $h \rightarrow \infty$ the Renyi entropy will vanish since spins will all point to the x -direction.

B. S_2 with three and four disjoint intervals

For completeness, we also consider dividing the system into more subregions. Now, we set the system with 24 sites, and divide it into six parts and eight parts respectively, please refer to the circles in the top-left corner of the two panels in Fig.4. The subsystem A contains the blue parts, i.e., $A = \cup_i a_i$, and the complement part B contains the red parts, i.e., $B = \cup_i b_i$ where $i = 1, 2, 3$ (for

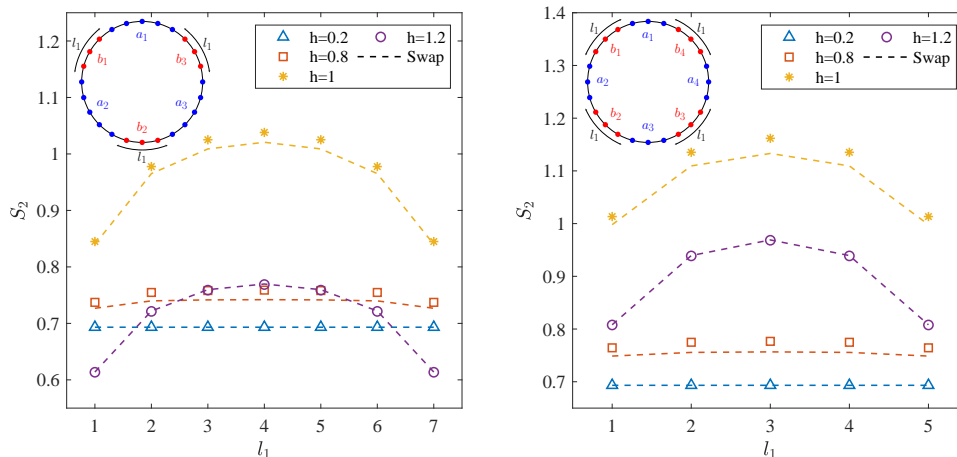


FIG. 4: (Left) Renyi entropy S_2 with three disjoint intervals $A = a_1 \cup a_2 \cup a_3$ against l_1 , the size of each b_i ($i = 1, 2, 3$). (Right) Renyi entropy S_2 with four disjoint intervals $A = a_1 \cup a_2 \cup a_3 \cup a_4$ against l_1 , the size of each b_i ($i = 1, 2, 3, 4$). In both panels, the circles in the top-left corners are the schematic pictures to show the arrangements of the disjoint intervals. Meanwhile, different styles of the points represent the Renyi entropy obtained from the machine learning methods with neural network for various magnetic fields, while the dashed lines correspond to the diagonalization of the Hamiltonian from the SVD method. They match each other very well within errors.

the left plot) or $i = 1, 2, 3, 4$ (for the right plot). For simplicity, we equally partition the subregions, which means that each a_i part has the same size and each b_i part has the same size as well. And we study the Renyi entropy S_2 by changing the size of b_i (denoted as l_1) with various magnetic field strength h . Similar to Fig.3, all the different styles of the points represent the numerical data from the machine learning methods, while the dashed lines represent the method from diagonalization of the Hamiltonian by SVD.

Obviously, from the left plot of Fig.4, there is a parity symmetry $l_1 \leftrightarrow (8 - l_1)$ due to the periodic boundary conditions and the equally partitioned subregions of a_i and b_i . In the same manner, the right plot of Fig.4 has a parity symmetry $l_1 \leftrightarrow (6 - l_1)$. As the magnetic field is close to zero such as $h = 0.2$, the Renyi entropies S_2 are roughly constants $\approx \ln 2$, which can be explained similarly as that in the preceding subsection. Then, as h increases, the Renyi entropies grow as well until the system arrives at the critical point of the phase transition. As h goes beyond the critical value $h_c = 1$, the entropies decrease again since the system enters into the paramagnetic phase. As expected, the entropies will vanish as $h \rightarrow \infty$.

$h \backslash l_1$	1	2	3	4
0.2	2.71×10^{-6}	4.02×10^{-6}	4.34×10^{-6}	4.41×10^{-6}
0.8	1.44×10^{-2}	2.01×10^{-2}	2.22×10^{-2}	2.28×10^{-2}
1.0	5.99×10^{-3}	1.29×10^{-2}	1.61×10^{-2}	1.70×10^{-2}
1.2	6.34×10^{-4}	9.82×10^{-4}	1.11×10^{-3}	1.22×10^{-3}

TABLE III: The relative errors ϵ between the machine learning methods and the SVD methods for computing S_2 with three disjoint intervals. The first row l_1 represents the size of b_i ($i = 1, 2, 3$), while the first column represents the magnetic field strength h . This table corresponds to the left plot of Fig.4.

$h \backslash l_1$	1	2	3
0.2	5.70×10^{-6}	7.42×10^{-6}	7.73×10^{-6}
0.8	2.09×10^{-2}	2.54×10^{-2}	2.64×10^{-2}
1.0	1.53×10^{-2}	2.32×10^{-2}	2.53×10^{-2}
1.2	4.90×10^{-4}	6.94×10^{-4}	6.32×10^{-4}

TABLE IV: The relative errors ϵ between the machine learning and the SVD methods for S_2 with four disjoint intervals. The first row l_1 is the size of b_i ($i = 1, 2, 3, 4$), and the first column is the magnetic field strength h . This table corresponds to the right plot of Fig.4.

From Fig.4 we see that the data points and the dashed lines match each other very well although at some points there are a little bit discrepancies. We list the relative errors ϵ in the Table III (corresponds to the left panel of Fig.4) and Table IV (corresponds to the right panel of Fig.4). From these two

tables we can see that the biggest error is roughly 2.64×10^{-2} in the Table IV for $h = 0.8$ and $l_1 = 3$. This error is still very small, therefore, we can confirm that the two methods (machine learning with neural networks and diagonalization of Hamiltonian with SVD) match each other within errors.

V. CONCLUSIONS AND DISCUSSIONS

We studied the second order Renyi entropy S_2 for the one-dimensional TFQIM with two, three and four disjoint intervals from the improved swapping operations. In particular, we have used two different methods to compute S_2 from the expectation values of the swapping operator $S_{\text{wap}}^{(2)}$. One method is the machine learning method with neural networks; The other one is the diagonalization of the Hamiltonian with SVD method. Consequently, we found that the results obtained from these two methods matched each other very well within errors, indicating that the machine learning methods with neural networks can be applied well in computing the Renyi entropy. By varying the magnetic field strength from smaller values to larger values, the phase of the spin chain will change from ferromagnetic to paramagnetic phase. From the results of Renyi entropy, we observed that as magnetic field was small, the value of S_2 was close to the constant $\ln 2$. This indicates that the system mainly exists two degenerated ground states with all spins point up or down. As the magnetic field increased, the Renyi entropy increased as well until the magnetic field arrived the critical point $h_c = 1$. In this case the system was in conformal field theory which could be analytically studied. Our results are consistent with the results from the conformal field theory as we have discussed in our recent paper [22]. However, as magnetic field exceeds the critical point, the phase of the system enters the paramagnetic phase. Therefore, the Renyi entropy will decrease as magnetic field goes beyond the critical value. As expected, if the magnetic field goes to infinity, the entropy will vanish since there will be only one configuration of the system. That is all the spins will point to the x -direction.

The first significance of our paper is that we can not only study the Renyi entropy with two disjoint intervals, but also we can investigate the Renyi entropy with more disjoint intervals, such as three and four intervals. The later cases are seldom studied in the existing literatures. The second significance of our paper is that we have used the state-of-the-art machine learning methods with neural networks to study the Renyi entropy with more disjoint intervals. The results obtained from the machine learning methods are consistent with those from the SVD method. We also found that in the case of Fig.3 with two disjoint intervals, the two methods match each other with high precision. However, in the case of Fig.4 with three and four disjoint intervals, the errors between the two methods become larger although the errors are still acceptable. We speculate that if there are too many disjoint intervals, the sampling approximations of the quantum states of the system from the machine learning methods may become not too accurate. The third significance of our paper is that our two methods can not only study the Renyi entropy at the critical point which is in conformal field theory, but also they can study the Renyi entropy beyond the critical regime. These two methods provide new avenues to study the Renyi entropy with multiple disjoint intervals.

Meanwhile, it should also be noted that the swapping operation for computing Renyi entropy is viable for various states, not limited to the ground states. For instance, it may apply in the excited states or in the dynamical states. In our paper we only focus on the second order Renyi entropy S_2 in the one-dimensional TFQIM model, however, in principle it can be extended to higher order Renyi entropy S_m in higher dimensions. We leave them for future work.

ACKNOWLEDGEMENTS

We greatly appreciate Prof. Jie Jiang for her indispensable financial support. This work was partially supported by the National Natural Science Foundation of China (Grants No.12175008).

Appendix A: Computational details of swapping operation

In this Appendix, we will show the computational details of arbitrary m -th order Renyi entropy S_m with n disjoint intervals, which can be found in the Supplemental Materials in our recent paper [22]. S_m is defined as,

$$S_m = \frac{1}{1-m} \ln \text{Tr}(\rho_A^m). \quad (\text{S.1})$$

The subsystem A is $A = \cup_i a_i$ while the complement part $B = \cup_i b_i$ ($i = 1, 2, \dots, n$). Their arrangements are like those in the preceding section, i.e., $a_1 b_1 a_2 b_2 \dots a_n b_n$. Under this partition, the wave function of the entire system can be represented as

$$|\Psi\rangle = \sum_{\mathbf{ab}} C_{a_1 b_1 \dots a_n b_n} \otimes_{i=1}^n (|a_i\rangle |b_i\rangle), \quad (\text{S.2})$$

in which $\sum_{\mathbf{ab}}$ means $\sum_{b_1 b_2 \dots b_n}^{a_1 a_2 \dots a_n}$ and $\otimes_{i=1}^n$ is the n times of the tensor product of the states $|a_i\rangle |b_i\rangle$.

To obtain the value of $\text{Tr}(\rho_A^m)$, one can construct the m -th order swapping operator $S_{\text{wap}}^{(m)}$ acting the m copies of the states of the system. The rule is like,

$$\begin{aligned} S_{\text{wap}}^{(m)} \otimes_{j=1}^m |\Psi^j\rangle &= S_{\text{wap}}^{(m)} \otimes_{j=1}^m \left[\sum_{\mathbf{a}^j \mathbf{b}^j} C_{a_1^j b_1^j \dots a_n^j b_n^j} \otimes_{i=1}^n (|a_i^j\rangle |b_i^j\rangle) \right] \\ &= \otimes_{j=1}^{m-1} \left[\sum_{\mathbf{a}^j \mathbf{b}^j} C_{a_1^j b_1^j \dots a_n^j b_n^j} \otimes_{i=1}^n (|a_i^{j+1}\rangle |b_i^j\rangle) \right] \otimes \left[\sum_{\mathbf{a}^m \mathbf{b}^m} C_{a_1^m b_1^m \dots a_n^m b_n^m} \otimes_{k=1}^n (|a_k^1\rangle |b_k^m\rangle) \right]. \end{aligned} \quad (\text{S.3})$$

In the above procedure, the swapping operator $S_{\text{wap}}^{(m)}$ has the effect of replacing the state $|a_i^{j+1}\rangle$ in the subsystem A^{j+1} in the $(j+1)$ -th replica, with the state $|a_i^j\rangle$ in the subsystem A^j in the j -th replica. This replacement is done for every two adjacent replicas. It should be noted that the subsystem A^1 of the first replica is replaced with the subsystem A^m of the last replica. This procedure is similar to the replica trick in quantum field theory as we have discussed in the main text.

Under this process, the expectation value of the swapping operator can be calculated as,

$$\begin{aligned} \langle S_{\text{wap}}^{(m)} \rangle &= \langle \otimes_{j'=1}^m \Psi^{j'} | S_{\text{wap}}^{(m)} | \otimes_{j=1}^m \Psi^j \rangle \\ &= \otimes_{j'=1}^m \left[\sum_{\mathbf{a}'^{j'} \mathbf{b}'^{j'}} C_{a_1^{j'} b_1^{j'} \dots a_n^{j'} b_n^{j'}}^* \otimes_{i'=1}^n (\langle a_{i'}^{j'} | \langle b_{i'}^{j'} |) \right] \otimes_{j=1}^{m-1} \left[\sum_{\mathbf{a}^j \mathbf{b}^j} C_{a_1^j b_1^j \dots a_n^j b_n^j} \otimes_{i=1}^n (|a_i^{j+1}\rangle |b_i^j\rangle) \right] \\ &\quad \otimes \left[\sum_{\mathbf{a}^m \mathbf{b}^m} C_{a_1^m b_1^m \dots a_n^m b_n^m} \otimes_{k=1}^n (|a_k^1\rangle |b_k^m\rangle) \right] \\ &= \prod_{j,j'=1}^{m-1} \sum_{\mathbf{a}^j \mathbf{b}^j} [C_{a_1^{j'} b_1^{j'} \dots a_n^{j'} b_n^{j'}}^* C_{a_1^j b_1^j \dots a_n^j b_n^j} \prod_{i=1}^n (\delta_{a_i^{j'} a_i^{j+1}} \delta_{b_i^{j'} b_i^j})] \\ &\quad \times \sum_{\mathbf{a}^m \mathbf{b}^m} [C_{a_1^m b_1^m \dots a_n^m b_n^m}^* C_{a_1^m b_1^m \dots a_n^m b_n^m} \prod_{k=1}^n (\delta_{a_k^m a_k^1} \delta_{b_k^m b_k^m})] \\ &= \prod_{j=1}^{m-1} \sum_{\mathbf{a}^j \mathbf{b}^j} [C_{a_1^{j+1} b_1^{j+1} \dots a_n^{j+1} b_n^{j+1}}^* C_{a_1^j b_1^j \dots a_n^j b_n^j}] \times \sum_{\mathbf{a}^m \mathbf{b}^m} [C_{a_1^1 b_1^1 \dots a_n^1 b_n^1}^* C_{a_1^m b_1^m \dots a_n^m b_n^m}]. \end{aligned} \quad (\text{S.4})$$

In order to verify $\text{Tr}(\rho_A^m)$ is equal to the expectation value of $S_{\text{wap}}^{(m)}$, we need to know the density matrix ρ of the whole system,

$$\rho = |\Psi\rangle \langle \Psi| = \sum_{\mathbf{abcd}} C_{a_1 b_1 \dots a_n b_n} C_{c_1 d_1 \dots c_n d_n}^* \otimes_{i=1}^n (|a_i\rangle |b_i\rangle) \otimes_{i'=1}^n (\langle c_{i'} | \langle d_{i'} |). \quad (\text{S.5})$$

Then, the reduced density matrix ρ_A for subsystem A is obtained by tracing out the subsystem B,

$$\begin{aligned}
\rho_A &= \text{Tr}_B(\rho) = \sum_{\mathbf{b}'} \otimes_{j=1}^n (\langle b'_j |) \rho \otimes_{j'=1}^n (|b'_{j'}\rangle) \\
&= \sum_{\mathbf{b}'} \sum_{\mathbf{abcd}} C_{a_1 b_1 \dots a_n b_n} C_{c_1 d_1 \dots c_n d_n}^* \otimes_{j=1}^n (\langle b'_j |) \otimes_{i=1}^n (|a_i\rangle |b_i\rangle) \otimes_{i'=1}^n (\langle c_{i'} | \langle d_{i'} |) \otimes_{j'=1}^n (|b'_{j'}\rangle) \\
&= \sum_{\mathbf{abcdb}'} C_{a_1 b_1 \dots a_n b_n} C_{c_1 d_1 \dots c_n d_n}^* \prod_{j=1}^n (\delta_{b'_j b_j}) \prod_{j'=1}^n (\delta_{d_{j'} b'_{j'}}) \otimes_{i=1}^n (|a_i\rangle) \otimes_{i'=1}^n (\langle c_{i'} |) \\
&= \sum_{\mathbf{abc}} C_{a_1 b_1 \dots a_n b_n} C_{c_1 b_1 \dots c_n b_n}^* \otimes_{i=1}^n (|a_i\rangle) \otimes_{i'=1}^n (\langle c_{i'} |). \tag{S.6}
\end{aligned}$$

Next, we need to calculate the m -th power of reduced density matrix ρ_A ,

$$\begin{aligned}
\rho_A^m &= \prod_{j=1}^m \left[\sum_{\mathbf{a}^j \mathbf{b}^j \mathbf{c}^j} C_{a_1^j b_1^j \dots a_n^j b_n^j} C_{c_1^j b_1^j \dots c_n^j b_n^j}^* \otimes_{i=1}^n (|a_i^j\rangle) \otimes_{i'=1}^n (\langle c_{i'}^j |) \right] \\
&= \prod_{j=1}^{m-1} \left[\sum_{\mathbf{a}^j \mathbf{b}^j \mathbf{c}^j} C_{a_1^j b_1^j \dots a_n^j b_n^j} C_{c_1^j b_1^j \dots c_n^j b_n^j}^* \prod_{i=1}^n (\delta_{c_i^j a_i^{j+1}}) \right] \\
&\quad \times \sum_{\mathbf{a}^m \mathbf{b}^m \mathbf{c}^m} \left[C_{a_1^m b_1^m \dots a_n^m b_n^m} C_{c_1^m b_1^m \dots c_n^m b_n^m}^* \otimes_{k=1}^n (|a_k^1\rangle) \otimes_{k'=1}^n (\langle c_{k'}^m |) \right] \\
&= \prod_{j=1}^{m-1} \left[\sum_{\mathbf{a}^j \mathbf{b}^j} C_{a_1^j b_1^j \dots a_n^j b_n^j} C_{a_1^{j+1} b_1^{j+1} \dots a_n^{j+1} b_n^{j+1}}^* \right] \\
&\quad \times \sum_{\mathbf{a}^m \mathbf{b}^m \mathbf{c}^m} \left[C_{a_1^m b_1^m \dots a_n^m b_n^m} C_{c_1^m b_1^m \dots c_n^m b_n^m}^* \otimes_{k=1}^n (|a_k^1\rangle) \otimes_{k'=1}^n (\langle c_{k'}^m |) \right]. \tag{S.7}
\end{aligned}$$

Then, the trace of ρ_A^m becomes,

$$\begin{aligned}
\text{Tr}(\rho_A^m) &= \prod_{j=1}^{m-1} \left[\sum_{\mathbf{a}^j \mathbf{b}^j} C_{a_1^j b_1^j \dots a_n^j b_n^j} C_{a_1^{j+1} b_1^{j+1} \dots a_n^{j+1} b_n^{j+1}}^* \right] \times \sum_{\mathbf{a}^m \mathbf{b}^m \mathbf{c}^m} \left[C_{a_1^m b_1^m \dots a_n^m b_n^m} C_{c_1^m b_1^m \dots c_n^m b_n^m}^* \prod_{k=1}^n (\delta_{a_k^1 c_k^m}) \right] \\
&= \prod_{j=1}^{m-1} \left[\sum_{\mathbf{a}^j \mathbf{b}^j} C_{a_1^j b_1^j \dots a_n^j b_n^j} C_{a_1^{j+1} b_1^{j+1} \dots a_n^{j+1} b_n^{j+1}}^* \right] \times \sum_{\mathbf{a}^m \mathbf{b}^m} \left[C_{a_1^m b_1^m \dots a_n^m b_n^m} C_{a_1^m b_1^m \dots a_n^m b_n^m}^* \right] = \langle S_{\text{wap}}^{(m)} \rangle. \tag{S.8}
\end{aligned}$$

From the Eq.(S.4) we see that the trace $\text{Tr}(\rho_A^m)$ is exact equal to $\langle S_{\text{wap}}^{(m)} \rangle$. Therefore, the computation of the m -th Renyi entropy S_m with n disjoint intervals is transformed to computing the expectation values of the swapping operator,

$$S_m = \frac{1}{1-m} \ln(\langle S_{\text{wap}}^{(m)} \rangle). \tag{S.9}$$

Appendix B: Machine learning methods with neural networks

1. Energy minimization with stochastic reconfiguration

For a given Hamiltonian H , the expectation value of energy can be estimated with neural network quantum state as

$$E(\mathcal{W}) = \frac{\langle \Psi_{NN}(\mathcal{W}) | H | \Psi_{NN}(\mathcal{W}) \rangle}{\langle \Psi_{NN}(\mathcal{W}) | \Psi_{NN}(\mathcal{W}) \rangle}. \tag{S.1}$$

Since the ground state has the lowest energy, for approximating the ground state, we can minimize the energy by optimizing \mathcal{W} with stochastic reconfiguration (SR) method. As we change the parameters slightly with $\mathcal{W}_k \rightarrow \mathcal{W}'_k = \mathcal{W}_k + \delta\mathcal{W}_k$, $k = 1, 2, 3 \dots p$, the new state can be expanded as

$$|\Psi'(\mathcal{W} + \delta\mathcal{W})\rangle = \delta\mathcal{W}_0|\Psi(\mathcal{W})\rangle + \sum_{k'=1}^p \delta\mathcal{W}_{k'} \frac{\partial}{\partial\mathcal{W}_{k'}} |\Psi(\mathcal{W})\rangle. \quad (\text{S.2})$$

In order to estimate the energy with configuration samples later, we can rewrite $|\Psi\rangle$ in the configuration representation, in which the configurations $|s\rangle$ are complete bases of the Hilbert space,

$$|\Psi'(\mathcal{W}')\rangle = \delta\mathcal{W}_0|\Psi(\mathcal{W})\rangle + \sum_{k'=1}^p \delta\mathcal{W}_{k'} \frac{\partial}{\partial\mathcal{W}_{k'}} \sum_s |s\rangle \langle s|\Psi(\mathcal{W})\rangle \quad (\text{S.3})$$

$$= \delta\mathcal{W}_0|\Psi(\mathcal{W})\rangle + \sum_{k'=1}^p \delta\mathcal{W}_{k'} \sum_s \frac{\partial \langle s|\Psi(\mathcal{W})\rangle}{\partial\mathcal{W}_{k'}} |s\rangle \quad (\text{S.4})$$

$$= \delta\mathcal{W}_0|\Psi(\mathcal{W})\rangle + \sum_{k'=1}^p \delta\mathcal{W}_{k'} \sum_s \frac{\partial \ln \langle s|\Psi(\mathcal{W})\rangle}{\partial\mathcal{W}_{k'}} |s\rangle \langle s|\Psi(\mathcal{W})\rangle. \quad (\text{S.5})$$

The variational derivatives with respect to the parameter \mathcal{W}_k can be defined as

$$\hat{\mathcal{O}}_k = \begin{cases} \mathbf{1}, & \text{for } k = 0 \\ \sum_s \frac{\partial \ln \langle s|\Psi(\mathcal{W})\rangle}{\partial\mathcal{W}_k} |s\rangle \langle s|, & \text{for } k \neq 0 \end{cases} \quad (\text{S.6})$$

Therefore, the new state can be rewritten as operator $\hat{\mathcal{O}}_k$ acting on the original state,

$$|\Psi'(\mathcal{W}')\rangle = \sum_{k'=0}^p \delta\mathcal{W}_{k'} \hat{\mathcal{O}}_{k'} |\Psi(\mathcal{W})\rangle. \quad (\text{S.7})$$

Next, we need to match the operator $\hat{\mathcal{O}}_k$ to a step of iterations which can decrease the energy of state. We can choose the power method introduced in [28] to act the operator $(\Lambda - H)$ repeatedly to the state, where Λ is a large enough number,

$$|\Psi(\mathcal{W})\rangle = \sum_{n=0}^{\infty} \langle n|\Psi(\mathcal{W})\rangle |n\rangle, \quad (\text{S.8})$$

$$(\Lambda - H)^N |\Psi(\mathcal{W})\rangle = \sum_{n=0}^{\infty} (\Lambda - E_n)^N \langle n|\Psi(\mathcal{W})\rangle |n\rangle. \quad (\text{S.9})$$

As $\Lambda > E_n$ for arbitrary n , the ground state will become dominant with iterations, since the energy of ground state E_0 is the minimum eigenenergy. In one iteration, we should represent the new state which is the state from the last iteration acted by the operator $(\Lambda - H)$. Therefore, we can change the parameters \mathcal{W} to match the changed state $|\Psi'(\mathcal{W}')\rangle$ and the new state,

$$|\Psi'(\mathcal{W}')\rangle = (\Lambda - H)|\Psi(\mathcal{W})\rangle = \sum_{k'=0}^p \delta\mathcal{W}_{k'} \hat{\mathcal{O}}_{k'} |\Psi(\mathcal{W})\rangle. \quad (\text{S.10})$$

Projecting the new state onto $\langle\Psi(\mathcal{W})|$ and $\langle\Psi(\mathcal{W})|\hat{\mathcal{O}}_k^\dagger$, we reach

$$\langle\Psi(\mathcal{W})|\hat{\mathcal{O}}_k^\dagger(\Lambda - H)|\Psi(\mathcal{W})\rangle = \sum_{k'=0}^p \langle\Psi(\mathcal{W})|\hat{\mathcal{O}}_k^\dagger \delta\mathcal{W}_{k'} \hat{\mathcal{O}}_{k'} |\Psi(\mathcal{W})\rangle, \quad (\text{S.11})$$

$$\langle\Psi(\mathcal{W})|(\Lambda - H)|\Psi(\mathcal{W})\rangle = \sum_{k'=0}^p \langle\Psi(\mathcal{W})|\delta\mathcal{W}_{k'} \hat{\mathcal{O}}_{k'} |\Psi(\mathcal{W})\rangle, \quad (\text{S.12})$$

in which the left-hand sides can be rewritten as

$$\Lambda \langle \hat{\mathcal{O}}_k^\dagger \rangle - \langle \hat{\mathcal{O}}_k^\dagger H \rangle = \langle \hat{\mathcal{O}}_k^\dagger \rangle \delta \mathcal{W}_0 + \sum_{k'=1}^p \langle \hat{\mathcal{O}}_k^\dagger \hat{\mathcal{O}}_{k'} \rangle \delta \mathcal{W}_{k'}, \quad (\text{S.13})$$

$$\Lambda - \langle H \rangle = \delta \mathcal{W}_0 + \sum_{k'=1}^p \langle \hat{\mathcal{O}}_{k'} \rangle \delta \mathcal{W}_{k'}, \quad (\text{S.14})$$

where $\langle \dots \rangle$ represents the expect value in the configuration s . From Eq.(S.14), we can obtain $\delta \mathcal{W}_0$ as

$$\delta \mathcal{W}_0 = \Lambda - \langle H \rangle - \sum_{k'=1}^p \langle \hat{\mathcal{O}}_{k'} \rangle \delta \mathcal{W}_{k'}. \quad (\text{S.15})$$

And substitute it into Eq.(S.13), we arrive at

$$\Lambda \langle \hat{\mathcal{O}}_k^\dagger \rangle - \langle \hat{\mathcal{O}}_k^\dagger H \rangle = \langle \hat{\mathcal{O}}_k^\dagger \rangle (\Lambda - \langle H \rangle) - \sum_{k'=1}^p \langle \hat{\mathcal{O}}_{k'} \rangle \delta \mathcal{W}_{k'} + \sum_{k'=1}^p \langle \hat{\mathcal{O}}_k^\dagger \hat{\mathcal{O}}_{k'} \rangle \delta \mathcal{W}_{k'}, \quad (\text{S.16})$$

$$\implies \langle \hat{\mathcal{O}}_k^\dagger \rangle \langle H \rangle - \langle \hat{\mathcal{O}}_k^\dagger H \rangle = \sum_{k'=1}^p (\langle \hat{\mathcal{O}}_k^\dagger \hat{\mathcal{O}}_{k'} \rangle - \langle \hat{\mathcal{O}}_k^\dagger \rangle \langle \hat{\mathcal{O}}_{k'} \rangle) \delta \mathcal{W}_{k'}. \quad (\text{S.17})$$

For convenience, we can define the generalized force f_k and covariance matrix $s_{kk'}$ as

$$f_k \equiv \langle \hat{\mathcal{O}}_k^\dagger H \rangle - \langle \hat{\mathcal{O}}_k^\dagger \rangle \langle H \rangle, \quad (\text{S.18})$$

$$s_{kk'} \equiv \langle \hat{\mathcal{O}}_k^\dagger \hat{\mathcal{O}}_{k'} \rangle - \langle \hat{\mathcal{O}}_k^\dagger \rangle \langle \hat{\mathcal{O}}_{k'} \rangle. \quad (\text{S.19})$$

Therefore, the change of the parameters can be obtained as

$$\delta \mathcal{W}_{k'} = \sum_k -(s^{-1})_{k'k} f_k. \quad (\text{S.20})$$

Now, we will show how to calculate the expectation values for neural network quantum state in the main text. First, the state can be described as

$$\Psi(s, \mathcal{W}) \equiv \langle s | \Psi(\mathcal{W}) \rangle = \exp \left[\sum_j a_j s_j \right] \prod_i 2 \cosh \left[b_i + \sum_j w_{ij} s_j \right]. \quad (\text{S.21})$$

The values of $\langle \hat{\mathcal{O}}_k \rangle$ and $\langle H \rangle$ can be calculated by summing up the local values of $\mathcal{O}_k(s)$ and $E_{loc}(s)$ for all configurations according to its weight $|\Psi(s)|^2 / \langle \Psi | \Psi \rangle$, where $\mathcal{O}_k(s)$ and $E_{loc}(s)$ are defined as,

$$\mathcal{O}_{a_j}(s) \equiv \frac{\partial \ln \Psi(s, \mathcal{W})}{\partial \mathcal{W}_{a_j}} = s_j, \quad (\text{S.22})$$

$$\mathcal{O}_{b_i}(s) \equiv \frac{\partial \ln \Psi(s, \mathcal{W})}{\partial \mathcal{W}_{b_i}} = \tanh[b_i + \sum_j w_{ij} s_j], \quad (\text{S.23})$$

$$\mathcal{O}_{w_{ij}}(s) \equiv \frac{\partial \ln \Psi(s, \mathcal{W})}{\partial \mathcal{W}_{w_{ij}}} = s_j \tanh[b_i + \sum_j w_{ij} s_j], \quad (\text{S.24})$$

$$E_{loc}(s) \equiv \frac{\langle s | H | \Psi(s, \mathcal{W}) \rangle}{\Psi(s, \mathcal{W})}. \quad (\text{S.25})$$

2. Metropolis Hastings algorithm

Since the number of configurations of the state is too large, we cannot calculate the expectation values accurately, instead we can only evaluate it through samples. Metropolis Hastings algorithm is an importance sampling method that can give an unbiased estimation of the expectation values [29].

In the beginning, we generate a random configuration. Then a series of configurations are produced from this random configuration by the rules that the new configuration is chosen by flipping one site in the old configuration randomly, and accepting it by the probability,

$$P_{\text{accept}}(s^i \rightarrow s^{i+1}) = \min \left(1, \left| \frac{\Psi(s^{i+1})}{\Psi(s^i)} \right|^2 \right) \quad (\text{S.26})$$

We can produce a Markovian chain of configurations by iterating the above operations. When the chain is long enough, the last configuration will not be affected by the initial choice, then we can add it to the sample. The frequency of configuration in the sample set obtained in this method will follow the probability $|\Psi(s)|^2 / \langle \Psi | \Psi \rangle$ from the quantum state.

-
- [1] M.A. Nielsen and I.L. Chuang, *Quantum computation and quantum information*, Cambridge university press (2010).
- [2] R. Horodecki, P. Horodecki, M. Horodecki and K. Horodecki, *Quantum entanglement, Reviews of modern physics* **81** (2009) 865.
- [3] A. Rényi, *On measures of entropy and information*, in *Proceedings of the fourth Berkeley symposium on mathematical statistics and probability, volume 1: contributions to the theory of statistics*, vol. 4, pp. 547–562, University of California Press, 1961.
- [4] E. Beadle, J. Schroeder, B. Moran and S. Suvorova, *An overview of renyi entropy and some potential applications, in 2008 42nd Asilomar Conference on Signals, Systems and Computers*, pp. 1698–1704, IEEE, 2008.
- [5] J. Fuentes and J. Gonçalves, *Rényi entropy in statistical mechanics, Entropy* **24** (2022) 1080.
- [6] M. Skórski, *Shannon entropy versus renyi entropy from a cryptographic viewpoint*, in *IMA International Conference on Cryptography and Coding*, pp. 257–274, Springer, 2015.
- [7] P. Calabrese and J. Cardy, *Entanglement entropy and conformal field theory, Journal of physics a: mathematical and theoretical* **42** (2009) 504005.
- [8] P. Calabrese, J. Cardy and E. Tonni, *Entanglement entropy of two disjoint intervals in conformal field theory, Journal of Statistical Mechanics: Theory and Experiment* **2009** (2009) P11001.
- [9] P. Calabrese, J. Cardy and E. Tonni, *Entanglement entropy of two disjoint intervals in conformal field theory: Ii, Journal of Statistical Mechanics: Theory and Experiment* **2011** (2011) P01021.
- [10] M. Fagotti and P. Calabrese, *Entanglement entropy of two disjoint blocks in xy chains, Journal of Statistical Mechanics: Theory and Experiment* **2010** (2010) P04016.
- [11] V. Alba, L. Tagliacozzo and P. Calabrese, *Entanglement entropy of two disjoint blocks in critical ising models, Physical Review B—Condensed Matter and Materials Physics* **81** (2010) 060411.
- [12] D. Ceperley and B. Alder, *Quantum monte carlo, Science* **231** (1986) 555.
- [13] M. Troyer and U.-J. Wiese, *Computational complexity and fundamental limitations? format?; to fermionic quantum monte carlo simulations, Physical review letters* **94** (2005) 170201.
- [14] G. Carleo, I. Cirac, K. Cranmer, L. Daudet, M. Schuld, N. Tishby et al., *Machine learning and the physical sciences, Reviews of Modern Physics* **91** (2019) 045002.
- [15] H.-Q. Shi and H.-Q. Zhang, *Measuring Renyi Entropy in Neural Network Quantum States*, [2308.05513](#).
- [16] R. Orús, *Tensor networks for complex quantum systems, Nature Reviews Physics* **1** (2019) 538.
- [17] M.B. Hastings, I. González, A.B. Kallin and R.G. Melko, *Measuring renyi entanglement entropy in quantum monte carlo simulations, Physical review letters* **104** (2010) 157201.
- [18] A.M. Zagoskin, *Quantum theory of many-body systems*, vol. 174, Springer (1998).
- [19] T. Nishioka, S. Ryu and T. Takayanagi, *Holographic entanglement entropy: an overview, Journal of Physics A: Mathematical and Theoretical* **42** (2009) 504008.
- [20] T. Faulkner, *The entanglement renyi entropies of disjoint intervals in ads/cft, arXiv preprint arXiv:1303.7221* (2013) .
- [21] M. Headrick, *Entanglement renyi entropies in holographic theories, Physical Review D—Particles, Fields, Gravitation, and Cosmology* **82** (2010) 126010.
- [22] H.-Q. Shi and H.-Q. Zhang, *A universal approach to Renyi entropy of multiple disjoint intervals*, [2411.18353](#).
- [23] S. Sachdev, *Quantum phase transitions, Physics world* **12** (1999) 33.
- [24] W.H. Greub, *Linear algebra*, vol. 23, Springer Science & Business Media (2012).

- [25] G. Carleo and M. Troyer, *Solving the quantum many-body problem with artificial neural networks*, *Science* **355** (2017) 602.
- [26] H.-Q. Shi and H.-Q. Zhang, *Learning topological defects formation with neural networks in a quantum phase transition*, *Commun. Theor. Phys.* **76** (2024) 055101 [[2204.06769](#)].
- [27] A. Fischer and C. Igel, *An introduction to restricted boltzmann machines*, in *Progress in Pattern Recognition, Image Analysis, Computer Vision, and Applications: 17th Iberoamerican Congress, CIARP 2012, Buenos Aires, Argentina, September 3-6, 2012. Proceedings 17*, pp. 14–36, Springer, 2012.
- [28] R. Rürger, *Implementation of the Variational Monte Carlo method for the Hubbard model*, Ph.D. thesis, Master's thesis, Goethe University Frankfurt, 2013.
- [29] S. Chib and E. Greenberg, *Understanding the metropolis-hastings algorithm*, *The american statistician* **49** (1995) 327.